On the Impact of Intraluminal Thrombus Mechanical Behavior in AAA Passive Mechanics

FABIÁN RIVEROS,[1] GIAMPAOLO MARTUFI,[2] T. CHRISTIAN GASSER,[3] and JOSE F. RODRIGUEZ-MATAS[1]

[1]Aragon Institute of Engineering Research, Universidad de Zaragoza, Saragossa, Spain; [2]Department of Civil Engineering, University of Calgary, Calgary, Canada; and [3]Department of Solid Mechanics, School of Engineering Sciences, Royal Institute of Technology (KTH), Teknikringen 8, 100 44 Stockholm, Sweden

(*Received 9 August 2014; accepted 24 January 2015; published online 31 January 2015*)

INTRODUCTION

An abdominal aortic aneurysm (AAA) is a gradual and permanent expansion of the aorta that develops between the renal arteries and the iliac bifurcations. Most AAAs remain asymptomatic during lifetime. However, elevated wall stress together with wall-weakening may trigger AAA rupture,[38] which is the 10th leading cause of death in American white men 65–74 years of age.[45] In order to prevent AAA rupture, elective repair (either surgical or endovascular) is offered and several indication criteria (symptoms, 5.5 cm aneurysm diameter,[33] 0.5 cm diameter expansion within 6 months,[21,25] *etc.*) are clinically used. Most recently, biomechanical rupture risk assessment has gained clinical attention.[8,10,12,18,26,48]

Most large (approximately 75% of clinically relevant AAAs[17]) AAAs contain an intraluminal thrombus (ILT),[16] i.e., a non-homogenous pseudo-tissue that develops from coagulated blood and adheres to the dilated aortic wall. An ILT may partially compensate for the hemodynamic effects linked to the aneurysmatic expansion of the infrarenal aorta. Specifically, ILT can restore the lumen of a distended aorta to a semi-normal size and helps carry blood pressure, i.e., it unloads the underlying wall from stress through a stress-cushioning effect.[4,6,19,24,27,40,43,51] The stress-cushioning effect may be compromised in fissured ILTs.[24] However, a thick ILT layer is also known to weaken the underlying AAA wall,[49] and it has also been suggested it increases AAA rupture risk. Specifically, clinical studies showed that a rapid increase of ILT volume relates to AAA rupture risk,[42] a thicker ILT layer accelerates AAA expansion,[3] and a large ILT leads to a higher risk for cardiovascular events.[30] In conclusion, because of the above mentioned

Address correspondence to Jose F. Rodriguez-Matas, Aragon Institute of Engineering Research, Universidad de Zaragoza, Saragossa, Spain. Electronic mail: jfrodrig@unizar.es

competition between stress-cushioning and wall-weakening effects, the role of ILT with respect to the risk of AAA rupture remains not very well understood and further studies are needed to draw sound conclusions.

In-vitro testing of ILT tissue from AAAs found isotropic and almost linear stress strain properties[3,11,29,50] that gradually change across radial direction.[10,50] Most recent data[29] identified two distinct ILT morphologies with different mechanical properties: (i) a multilayered ILT whose strength and stiffness may either decrease gradually from the luminal to the medial/abluminal layer or decrease abruptly between the luminal and medial/abluminal layer; (ii) a single layer ILT, a newly formed thrombus, with a significantly lower strength and stiffness than the multi-layered ILT.

The reported wide variability of stiffness and strength for ILT tissue suggests considering this information in a biomechanical AAA rupture risk assessment. In addition, earlier results from our group[35,36] indicated that peak wall stress (PWS) was predominantly located at the ILT-free aneurysm wall, suggesting that, beside the specific ILT morphology (constitution), its topology (geometrical configuration) also considerably influences PWS predictions. This conclusion is in basic agreement with many other studies[15,20,24,27,32,51] that observed a considerable change of wall stress magnitude and distribution when incorporating ILT in a biomechanical analysis.

For the present work, 21 small AAAs were reconstructed from computer tomography (CT) data and biomechanically analyzed in order to uncover potential mechanisms by which ILT morphology and topology influence PWS. The employed FE models considered AAA wall anisotropy, used zero-pressure configuration as a stress-free reference configuration,[35] and assumed hypothetical arrangements of fibrotic and newly-formed ILT of reported stiffness.[3,11]

METHODS

Image Acquisition and 3D Reconstruction

In total, CT images of 21 non-ruptured patient-specific AAAs from two hospitals in Stockholm, Sweden, with maximum diameters between 4.2 and 5.4 cm have been considered for this study. A local ethics committee approved the use of anonymized human data, and the quality of CT images allowed accurate individual AAA models to be built. Images were reconstructed with diagnostic software A4clinics Research Edition (VASCOPS GmbH, Graz, Austria), which was applied by an operator with an engineering background and assisted by a radiologist to ensure a proper segmentation of aneurysms. Details regarding the image segmentation process are given elsewhere.[1] All reconstructed models included ILT and assumed a non-homogeneous aneurysm wall thickness that varied between 1.5 mm at the thrombus-free wall and 1.13 mm at sites covered by a thick (>25 mm) thrombus layer.[23] Reconstructed surfaces were exported in STereoLithography (STL) file format for further processing. Table 1 summarizes the main geometric characteristics of the considered AAAs.

Material Models

Constitutive Framework

In order to describe the finite strain kinematics we used multiplicative decomposition of the deformation gradient $\mathbf{F} = \mathbf{F}_{vol}\bar{\mathbf{F}}$ (with $J = \det\mathbf{F} > 0$) into volumetric $\mathbf{F}_{vol} = J^{+1/3}\mathbf{I}$ (with $J = \det\mathbf{F}_{vol}$) and an isochoric $\bar{\mathbf{F}} = J^{-1/3}\mathbf{F}$ (with $\det\bar{\mathbf{F}} = 1$) parts. In addition, the existence of a strain-energy function (SEF) W, i.e., from which the stress–strain response of the material can be derived, was postulated. Specifically, a transverse isotropic formulation was considered, where $\mathbf{a}_0$ denotes the principal anisotropy direction. Consequently, the transverse isotropic SEF has decoupled structure

$$W(\boldsymbol{C}, \mathbf{a}_0) = U(J) + \overline{W}(\bar{I}_1, \bar{I}_2, \bar{I}_4), \tag{1}$$

where $\mathbf{C} = \mathbf{F}^T\mathbf{F}$ is the right Cauchy-Green tensor. The volumetric elastic response U and isochoric elastic response $\overline{W}$ of the material are given scalar-valued functions of J and the invariants $\bar{I}_1, \bar{I}_2, \bar{I}_4$, of the modified right Cauchy-Green tensor $\bar{\mathbf{C}} = \mathbf{J}^{-2/3}\mathbf{C}$, and $\mathbf{a}_0$ according to

$$\bar{I}_1 = \mathrm{tr}\bar{\mathbf{C}}, \quad \bar{I}_2 = \frac{1}{2}\left[(\mathrm{tr}\bar{\mathbf{C}})^2 - \mathrm{tr}\bar{\mathbf{C}}^2\right], \quad \bar{I}_4 = \mathbf{a}_0 \cdot \bar{\mathbf{C}} \cdot \mathbf{a}_0. \tag{2}$$

From the particular SEF (1) the second Piola–Kirchoff stress tensor reads[41]

$$\mathbf{S} = Jp\mathbf{C}^{-1} + 2J^{-2/3}\sum_{\substack{i=1 \\ i\neq 3}}^{4} \frac{\partial \bar{W}}{\partial \bar{I}_i}\mathrm{DEV}\left(\frac{\partial \bar{I}_i}{\partial \bar{\mathbf{C}}}\right), \tag{3}$$

where $p = {}^{dU}/_{dJ}$ is the hydrostatic pressure, and $\mathrm{DEV}(\cdot) = (\cdot) - \frac{1}{3}[(\cdot) : \mathbf{C}]\mathbf{C}^{-1}$ is the deviator operator in the Lagrangian description. Finally a weighted push-forward defines the Cauchy stress tensor

$$\boldsymbol{\sigma} = J^{-1}\mathbf{F}\mathbf{S}\mathbf{F}^T. \tag{4}$$

AAA Wall Model

For the AAA wall the principal anisotropy direction $\mathbf{a}_0$ denotes the circumferential vessel direction and the tissue was modeled by the SEF[35]

TABLE 1. Characteristics of AAA models.

Model	Max diameter (cm)	Total AAA volume (cm^3)	Total ILT volume (cm^3)	Lumen diameter (cm)	Arterial wall elements	ILT elements	Total elements
B1	4.20	63,18	23.80	2.40	336,766	242,191	578,957
B2	5.06	104,03	48.20	3.05	285,509	291,834	577,343
B3	5.00	88,37	53.60	2.65	287,576	199,300	486,876
B4	5.42	79,78	40.20	2.30	346,193	288,170	634,363
B5	5.14	86,23	61.80	2.60	308,788	239,911	548,699
B6	4.80	117,05	65.92	2.30	338,181	213,913	552,094
B7	5.10	148,21	76.10	3.00	333,169	279,490	612,659
B8	4.70	101,45	36.80	3.60	292,151	282,051	574,202
B9	5.14	102,88	19.30	3.50	526,225	390,292	916,517
B10	4.69	101,61	32.50	2.30	471,006	454,455	925,461
B11	4.96	124,14	37.30	3.00	542,548	464,363	100,6911
B12	4.95	77,42	29.80	3.00	371,334	272,154	643,488
B13	4.57	92,68	28.10	3.20	448,897	408,567	857,464
B14	4.66	125,24	35.50	3.00	634,232	369,926	100,4158
B15	4.80	86,73	39.10	2.80	370,222	346,075	716,297
B16	4.67	100,13	19.40	3.95	561,545	400,480	962,025
B17	5.35	137,36	55.50	2.95	582,862	547,318	113,0180
B18	5.31	146,33	19.70	3.60	727,384	321,940	104,9324
B19	5.11	76,21	3.90	4.15	577,949	147,151	725,100
B20	4.88	93,58	66.60	1.75	436,167	335,403	771,570
B21	5.26	111,50	52.20	3.30	455,792	386,573	842,365
Mean ± SD	4.94 ± 0.30	103.05 ± 23.22	40.27 ± 18.69	2.97 ± 5.93	–	–	–

$$W_{wall}^{aniso} = \kappa(J-1)^2 + D_1\left(e^{D_2(\bar{I}_1-3)} - 1\right) + \frac{k_1}{k_2}\left(e^{k_2(\bar{I}_4-1)^2} - 1\right), \quad (5)$$

where $D_1 = 0.214$ kPa, $D_2 = 41.3$, $k_1 = 0.212$ kPa, $k_2 = 130$ are material parameters.[35] This equation reflects experimental data from the biaxial AAA wall characterization,[46] i.e., the tissue's properties are stiffest along the circumferential direction, i.e., the direction specified by $\mathbf{a}_0$. We also note that our material model does not distinguish between distinct wall layers, which is justified by similar collagen structures in the medial and adventitial layers of AAA wall.[9]

AAA ILT Model

For ILT we have considered two extreme cases: (i) a stiff thrombus tissue named as type A ILT; and (ii) a more compliant thrombus named as type B ILT. In addition, ILT tissue is regarded isotropic, i.e., constitutive formulations are independent of the principal anisotropy direction $\mathbf{a}_0$.

For type A, the SEF proposed by Di Martino and Vorp[5] has been used:

$$W_{TA} = C_{20}(\bar{I}_2 - 3) + C_{02}(\bar{I}_2 - 3)^2, \quad (6)$$

where C_{20} and C_{02} are material constants with dimensions of stress, and $\bar{I}_2$ is the second modified invariant. The reported parameters used were $C_{20} = 28$ kPa and $C_{02} = 28.6$ kPa.[5]

For type B ILT, representing a more compliant ILT tissue, we have used SEF proposed in the study by Gasser *et al.*[11]

$$W_{TB} = c\sum_{i=1}^{3}(\lambda_i^4 - 1), \quad (7)$$

where material parameter $c = 2.11$ kPa is the average of the luminal, medial, and abluminal ILT;[11] λ_i, $i = 1$, 2,3 denotes the ith principal stretch, which describes tissue elongation along the ith principal direction. Figure 1a shows Cauchy stress vs. strain for both types of ILT considered.

We note that SEF for ILT proposed by Di Martino and Vorp, and Gasser *et al.* are based on uniaxial testing instead of biaxial testing, as is the case for the arterial wall. However, previous studies on ILT luminal layer have demonstrated the tissue to be isotropic. As such, uniaxial testing should (theoretically) give the same results as biaxial testing. A comparison of luminal ILT's elastic behavior under uniaxial elongation according to two different constitutive models: (i) Gasser *et al.*[11] (from uniaxial testing) and (ii) van de Geest *et al.*[47] (from biaxial testing) gives the result shown in Fig. 1b. Given the variability of ILT properties, the mechanical response can be considered the same.

Finite Element Models

The geometric model for each patient was meshed with linear tetrahedrons and nearly isotropic meshes. The total number of elements per AAA model ranged

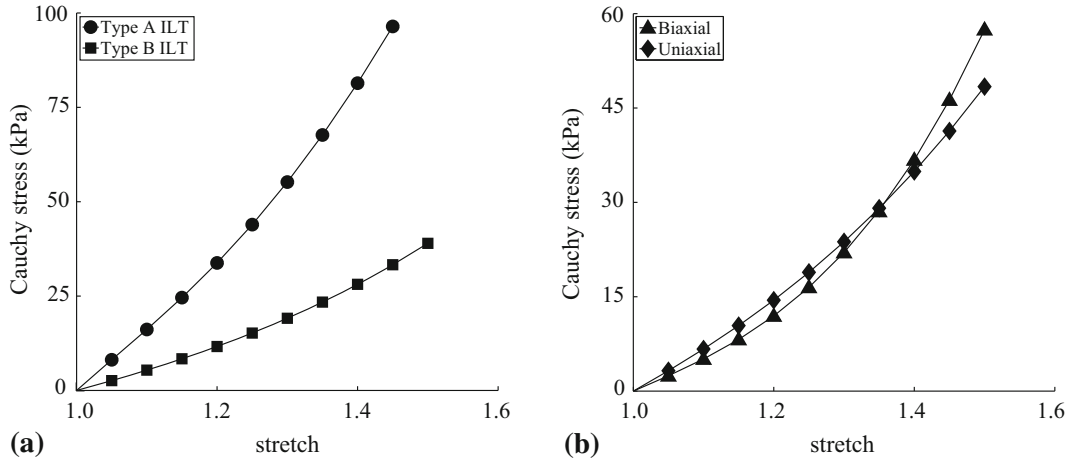

FIGURE 1. (a) Cauchy stress vs. stretch curves for the ILT material models considered in the study. (b) Comparison of luminal ILT's elastic behavior under uniaxial elongation according to two different constitutive models characterized using uniaxial test data[11] and biaxial test data.[47]

between 486 and 1130 k elements, and had at least three elements through the arterial wall thickness in order to capture the stress gradients through the wall. In addition, a sensitivity analysis of the mesh, as described previously,[35] was performed to ensure stress results independent from the discretization. In this regard, independence of average quantities, i.e., mean wall stress and mean ILT stress, were also checked. Table 1 summarizes the geometric characteristics and mesh sizes used for the 21 AAAs.

FE simulation was carried out in ABAQUS (Dassault Systèmes Simulia Corp.). The anisotropic material model for the AAA wall was implemented as a user subroutine UANISOHYPER_INV, whereas the ILT material models used the software's standard material libraries. The principal anisotropy direction $\mathbf{a}_0$ was defined as described in our previous work.[35]

Unfortunately, we did not have access to patient-specific intraluminal blood pressure and instead used mean diastolic and systolic arterial pressures of 80 mmHg (10.6 kPa) and 120 mmHg (16.0 kPa), respectively, for all our cases. The diastolic pressure was used during the iterative algorithm to find the zero-pressure configuration,[35] as the recorded images characterize this state of loading. The systolic pressure was used to find the largest stresses in the AAA wall. The constraints due to the thoracic aorta and common iliac arteries were simulated by restraining the longitudinal displacement while allowing displacements in radial direction.

We note that the aneurysmal model considers uniform mechanical properties, and we made no distinction between the aneurysm and the adjacent vasculature. In addition, residual stresses in zero-pressure configuration have been neglected and no contact with surrounding organs was considered. A refined model should consider the variation in the mechanical properties between the arterial and aneurysmal tissues as well as AAA wall heterogeneities.[44] However, as in the case of ILT tissue, this information was not available from CT images.

The developed FE models were equipped with different ILT models that aim to capture ILT variability with respect to morphology and topology. In addition FE models that completely neglect ILT were used for reference wall stress predictions.

Stress for the arterial wall are reported as peak maximum principal wall stress (PWS) and as average stress (MPWS) calculated as

$$MPWS = \frac{1}{V}\int_V \sigma_{III} dV, \tag{8}$$

where V is AAA tissue volume and σ_{III} is maximum principal stress. For ILT, peak, and average stresses refer to von Mises stress.

Statistical Analysis

Statistical analyses were performed in Matlab R2012 v.8.0, and data are reported by their mean and standard deviation (mean ± SD), respectively. The Lilliefors test was used to test the normality of the data. Statistical significance was tested with the Wilcoxon signed-rank test, where a two-sided p value of less than 0.05 determined significance. Finally, linear correlations among parameters were quantified by Pearson's linear correlation coefficient ρ.

RESULTS

FE models equipped with homogeneous ILT properties predicted PWS of 405 kPa (SD 168 kPa) and

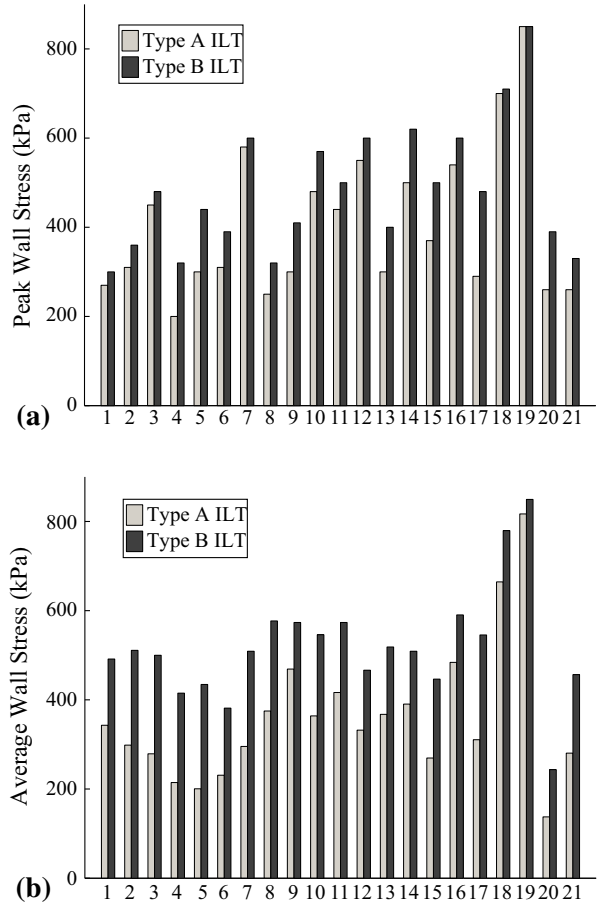

FIGURE 2. (a) Predicted peak principal stresses in the AAA wall; (b) Predicted average principal wall stress in the wall. Results use the zero pressure geometries for their stress-free reference configurations. Predictions are for type A ILT (light gray bars) and for type B ILT (dark gray bars).

484 kPa (SD 143 kPa) for type A and type B ILT material models, respectively. Both stress values are significantly lower than the failure stress reported in the literature for electively repaired aneurysms,[3] i.e., 820 kPa (SD 90 kPa). In all analyzed cases PWS was found to be higher for the model using the softer (type B) ILT material model, see Fig. 2a. The influence of ILT material behavior on AAA stress field becomes clearer when considering MPWS. In this case, the two groups (type A and type B) are clearly distinguishable, see Fig. 2b. Both PWS ($p < 0.001$) and MPWS ($p < 0.001$) were different for simulations using type A and type B ILT models.

Unlike what was found for wall stress, average stress in ILT was higher for type A than for type B thrombus ($p < 0.001$), see Fig. 3. This result is consistent with the larger compliance of type B ILT. For both ILT model types, predicted average stress was lower than the experimentally identified rupture stress

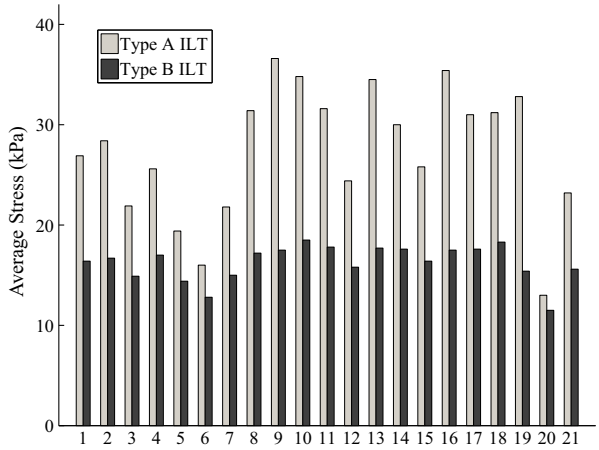

FIGURE 3. Predicted average von Mises stress in the ILT. Results use the zero pressure geometries for their stress-free reference configurations. Predictions are for type A ILT (light gray bars) and for type B ILT (dark gray bars).

of ILT[11] [type A: 156 kPa (SD 57.9); type B: 47.7 kPa (SD 22.9)].

Correlations of PWS and MPWS with AAA diameter and ILT volume are shown in Fig. 4. Although PWS somehow increases with diameter, no significant correlation between both variables is seen for any type of ILT (type A: $\rho = 0.09$, $p = 0.69$; type B: $\rho = 0.15$, $p = 0.51$). On the contrary, borderline significance was seen for correlation with ILT volume (type A: $\rho = -0.44$, $p = 0.05$; type B: $\rho = -0.40$, $p = 0.07$). Similar to PWS, no correlation of MPWS was seen when tested against diameter (type A: $\rho = 0.05$, $p = 0.82$; type B: $\rho = 0.15$, $p = 0.52$). However, a strong correlation between MPWS and ILT volume was found (type A: $\rho = -0.77$, $p < 0.001$; type B: $\rho = -0.69$, $p = 0.001$) indicating the significant influence of ILT on wall stress in AAAs.

In order to further investigate the influence of ILT on wall stress predictions, stress results with the different ILT models were compared to predictions from FE models that completely neglected the ILT. Specifically, the stress ratio between maximum principal stress (von Mises stress for ILT) from simulations without ILT and with a particular ILT model (type A or type B) was computed for each element of the AAA model, see Fig. 5.

Figure 5 clearly illustrates that a stiffer ILT model (type A) leads to a significantly higher stress reduction than the more compliant ILT model (type B) for all AAA cases. It is also noted that for AAA with thin ILTs, e.g., models 9, 16, and 19, a similar maximum stress ratio for both ILT types is obtained. In particular, case 19 has almost no ILT. Therefore, stress predictions from all models (type A, type B, and no ILT) are similar.

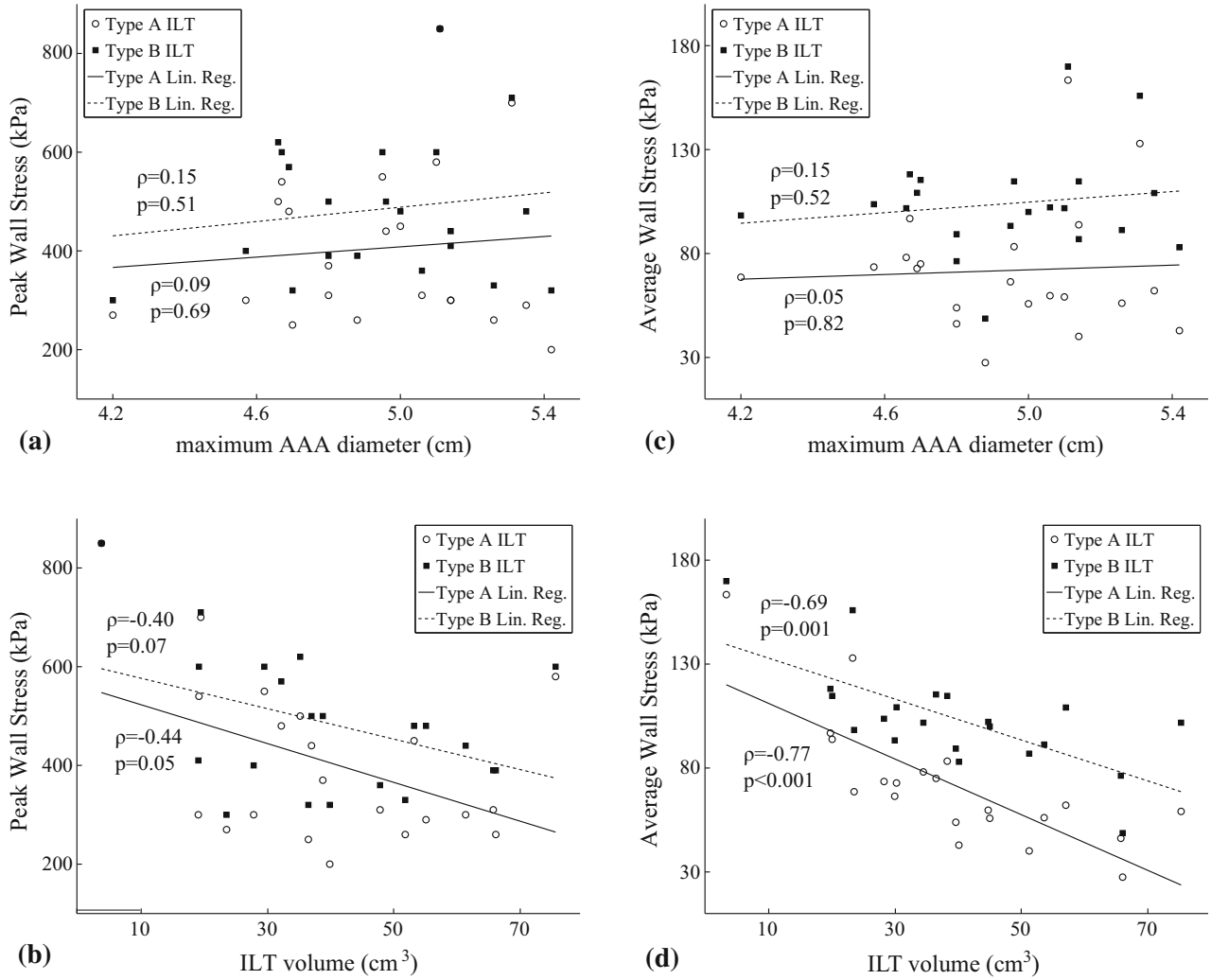

FIGURE 4. Predicted maximum principal wall stress (panels a and b) and average maximum principal wall stress (panels c and d) in the AAA wall for both types of ILT material compared to the maximum AAA diameter (panels a and c), and the ILT volume (panels b and d). Results use the zero pressure geometries for their stress-free reference configurations. The trend line shows a slight increase of the PWS with AAA maximum diameter, whereas PWS shows a tendency to decrease with ILT volume. The observed trend is the same for both ILT types.

In addition to the results shown in Fig. 5, it is noted that stress reduction is clearly limited to the sites that are covered by ILT while ILT-free parts of the wall remain exposed to the same stress that was predicted by ILT-free FE models. This observation is illustrated for case 1 by the inset of Fig. 5 and also hold for all other cases.

A closer analysis of the stress field obtained for each of the models (see Fig. 6) suggests that topology of ILT may play a more important role on PWS than ILT. Figure 6 shows maximum principal stress using type A ILT for 20 models (model 19 has been excluded because it is almost free of ILT). This figure indicates that PWS, in the lesion, seems to be located in the area corresponding to ILT-free parts of the wall. In fact, a detailed analysis of different sagittal sections of the models revealed that PWS was located in areas with minimum ILT thickness. This observation also hold when using type B ILT, and explains the good correlation between PWS and minimum ILT thickness shown in Fig. 7a (type A: $\rho = -0.73$, $p < 0.001$; type B: $\rho = -0.62$, $p = 0.002$). In addition, for the section where PWS is located we have found a strong correlation between PWS and Laplace's law computed using the effective lumen diameter and the effective wall thickness, $D_{\text{lumen}}/\left(t_{\text{wall}} + t_{\text{ILT}}^{\min}\right)$ (type A: $\rho = 0.87$, $p < 0.001$; type B: $\rho = 0.81$, $p < 0.001$). Here, D_{lumen} denotes the lumen diameter at the section of minimum ILT thickness, $t_{\text{ILT}}^{\min}$, and t_{wall}, is the local effective wall thickness at this site.

Current state of the art assumes homogeneous ILT properties in the simulations since heterogeneity is not available from CT scans. However, as demonstrated in previous studies,[11,29] ILT is heterogeneous with a stiff

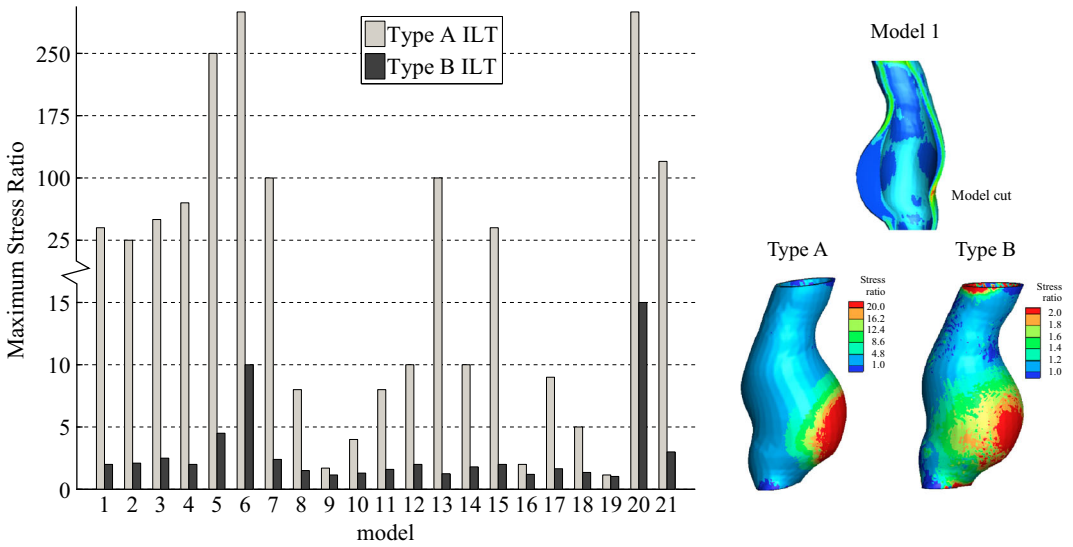

FIGURE 5. Predicted maximum stress ratio in the AAA wall covered by the ILT due to the presence of the ILT. Predictions are for type A ILT (light gray bars) and for type B ILT (dark gray bars). The inset shows the stress ratio profile for model 1. The maximum stress ratio located in the area of maximum ILT thickness.

and highly resistant lumen layer and a weaker and compliant medial-abluminal layer. Due to missing information regarding the spatial composition of ILT, our remaining analysis was based on a hypothetical model that allocates only stiff AAA tissue (modeled as type A ILT material) and more compliant AAA tissue (modeled as type B ILT material) as shown in Fig. 8. In addition, Fig. 8 shows the average AAA wall stress (MPWS) and the average ILT stresses as a function of the volume percentage of type A ILT. The top panel indicates a reduction of the average wall stress to a steady value as the percentage of type A ILT increases. On the contrary, average ILT stress increases monotonically, but slowly, with the percentage of type A ILT. It is noted that ILT stress behavior is more complex when distributed within the different layers (luminal and medial/abluminal layers), see Fig. 8b. While average stress in the type A ILT layer (in the luminal side) shows a non-monotonic behavior, the average stress in type B ILT layer (medial/abluminal layer) decreases monotonically with the percentage of type A ILT. This indicates that the stiffer layer of the ILT bears most of the ILT load.

DISCUSSION

The importance of ILT on AAA mechanics has attracted the attention of researchers for a long time. Most studies have focused on characterizing the mechanical properties of the ILT under static and dynamic (fatigue) conditions,[3,11,22,29,47] the association of ILT with hypoxia and aneurismal growth.[40,42,49] In addition some studies investigated the effect of ILT on wall stress.[5,10,15,31,32,51] In this regard, Di Martino and Vorp[5] studied the variation of ILT material properties on idealized geometries, but no conclusive studies are available on patient-specific geometries. The present study used 21 patient-specific AAA cases to investigate the impact of ILT mechanical properties and topology on PWS of patient-specific AAA geometries under static conditions. Specifically, state-of-the-art modeling assumptions were used, such as finite strains, anisotropy of the AAA wall and the zero-pressure configuration for all computations. ILT constitutions was represented through two extreme conditions: a firm and compact ILT tissue (type A), and a softer and more compliant ILT tissue (type B).[29] Finally, the influence of ILT heterogeneity on stress distributions was studied using idealized compositions of compact and soft ILT tissues.

The present study found a statistically significant influence of ILT's mechanical properties on PWS and MPWS, and therefore potentially also on AAA rupture risk. This is partially supported by the fact that variations in PWS and MPWS are much stronger correlated with ILT volume than with maximum AAA diameter. A finding that is in agreement with previous studies.[15,24,40] Consequently, for AAAs of similar diameter, ILT topology and composition seems to modulate the stress field in the AAA arterial wall. Clearly, other geometrical factors such as AAA size,[7,13,20,26,34,37,39] asymmetry,[7,16,37,39] wall curvature,[7,13,20,34,39] *etc.* also influence wall stress, and to what extent ILT topology is linked to them could not be investigated in the present study.

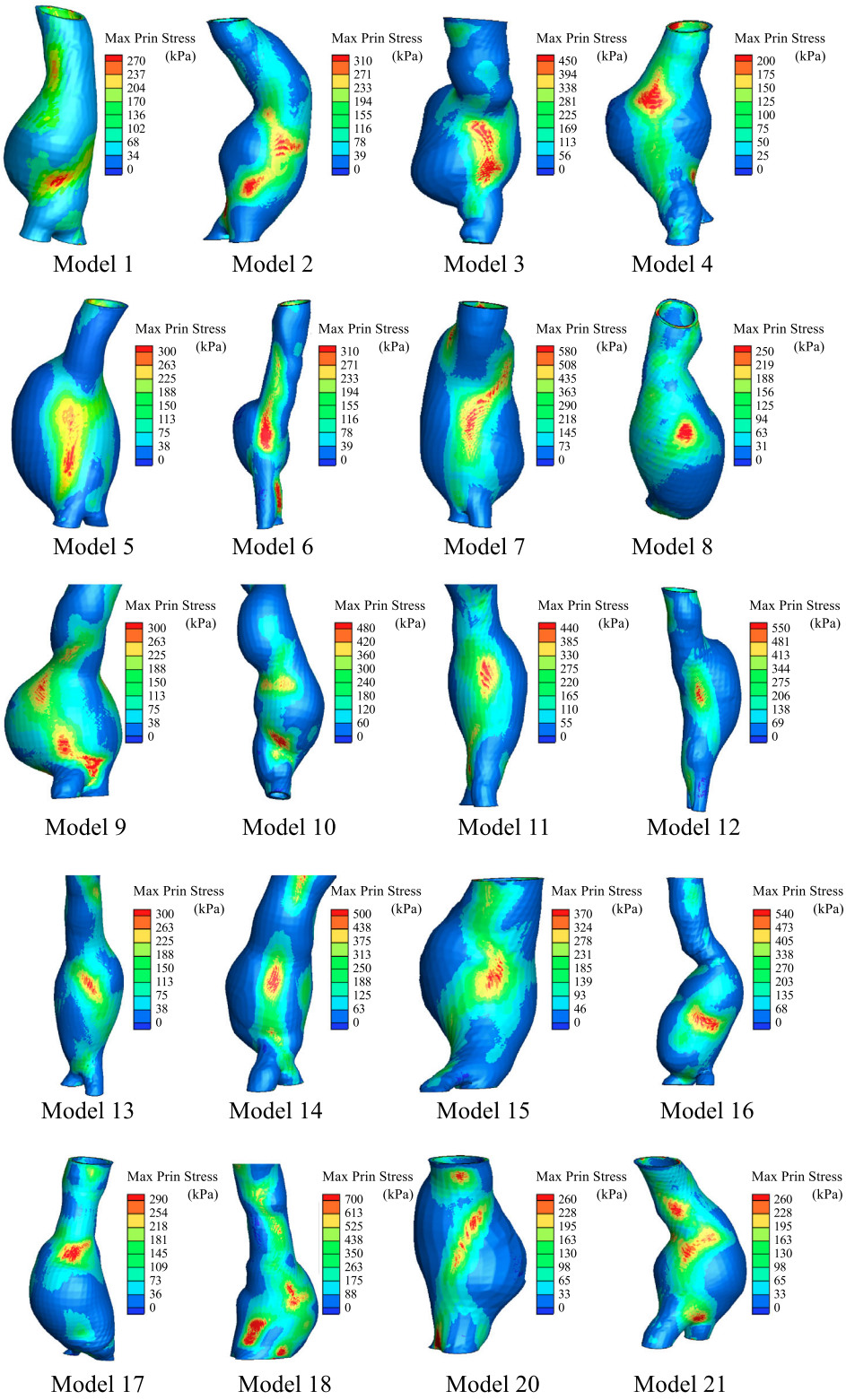

FIGURE 6. Stress field in the AAA models with asymmetric ILT. PWS was always located in the side where ILT thickness is minimum. Results correspond to type A ILT.

In all cases with ILT ($n = 20$), the location of PWS coincided with the section of minimum ILT thickness, and PWS correlated with the minimum ILT thickness ($\rho < -0.73$ $p < 0.001$). This suggests that ILT topology dictates the location of the PWS. Moreover, a remarkable correlation ($\rho > 0.87$; $p < 0.001$) was

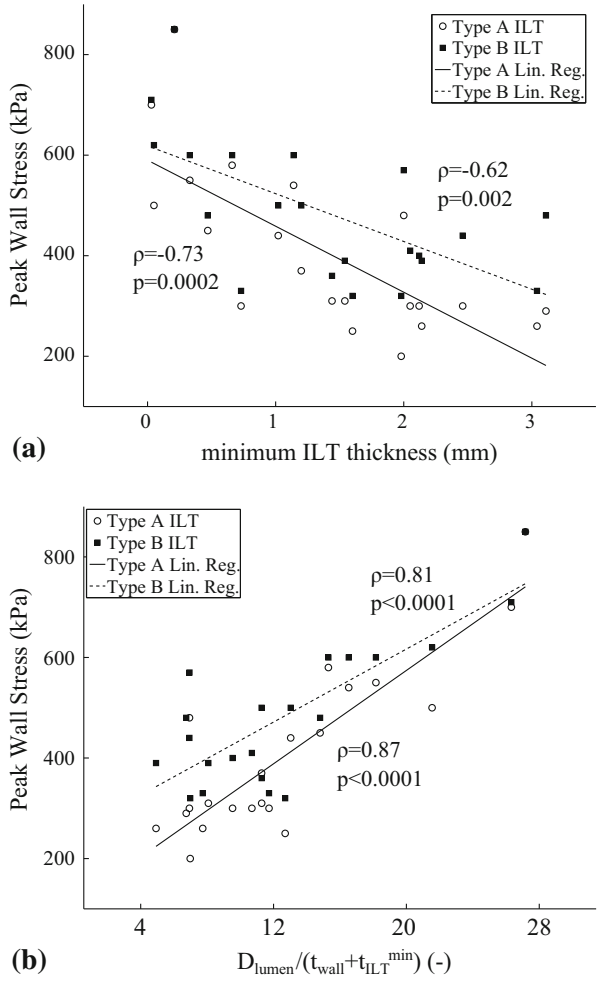

FIGURE 7. Peak Wall Stress for both ILT types. (a) As a function of minimum ILT thickness; (b) As a function of the local lumen diameter to wall thickness plus minimum ILT thickness ratio.

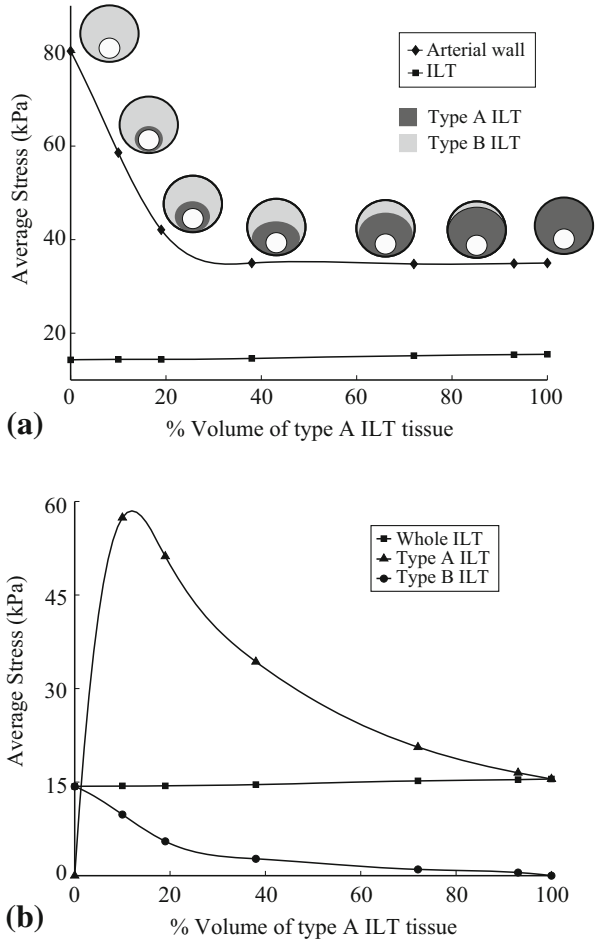

FIGURE 8. Average stress for a hypothetical heterogeneous ILT. Heterogeneity is represented as volume percentage of type A ILT tissue (section in dark gray in the top panel). (a) Mean stress in the arterial wall (solid line with solid diamonds) and ILT (solid line with solid squares); (b) Mean stress in ILT (solid line with solid squares) and in the individual ILT components: type B ILT (solid line with solid circles) and type A ILT (solid line with solid triangles).

found between PWS and the ratio between the effective lumen diameter and the stress-carrying structure thickness, i.e., minimum ILT thickness plus the local arterial wall thickness. This demonstrates that PWS in these cases is mainly determined by membrane type of loading, i.e., following Laplace's law. This result suggests that, in addition to maximum AAA diameter, particular attention should be paid to effective lumen diameter and minimum effective AAA thickness (wall + ILT thickness) when evaluating AAA risk.

Regarding the mechanical properties of the ILT, our results show that, for the same ILT geometry, a more compliant ILT leads to higher wall stress than a less compliant ILT. Consequently, a stiffer ILT is associated with a more pronounced reduction in wall stress than a more compliant ILT. Note also that the aneurysm wall is remarkably weaker and thinner[22,49] behind (thick) ILT when compared to the ILT-free wall. While the formation of new thrombus is a fast process, remodeling of the wall is determined by collagen turn-over, i.e., at a half-life time of about 2 months.[28] Consequently, since the AAA wall might be stronger behind a newly formed (soft) ITL than behind an older fibrotic (stiff) ILT, the less pronounced stress reduction effect due to the soft thrombus should not be seen directly as an increased risk of AAA rupture. Moreover, our results indicate that stress reduction in the wall when an ILT is present corresponds to an overall increase in AAA stiffness due to the presence of the ILT, which can be several times thicker than the wall, rather than a direct impact of the ILT's mechanical stiffness.

ILT heterogeneity markedly affected the stress field in the wall and ILT in our idealized study. While the mean stress in wall and the ILT varied monotonically as the percentage of the stiffer layer increased,

remarkably different behavior was found for the individual layers in the ILT. Most interestingly, the stiffer layer in a heterogeneous ILT was found to carry most of the load within the ILT. In fact, the simulations indicate that the mean stress in the stiffer layer may be larger than the mean stress in the wall. Since the strength of the luminal layer is considerably lower than the arterial wall,[3,11] these results suggest that failing of the luminal layer could occur in a heterogeneous ILT before the wall fails. Previous studies have suggested failure of ILT tissue as a cause of AAA rupture.[14,32]

Several limitations are associated with this study. At the moment of the study, we did not have access to patient-specific blood pressures and mean population values were used instead. However, conclusions drawn regarding the influence of ILT mechanical properties and morphology on AAA biomechanics should be almost independent from this limitation. Not considering the poroelastic nature of the ILT is another study limitation.[2,19,31] A recent study reports that including the poroelastic description of a homogeneous ILT does not change the computed arterial wall stress that was predicted with hyperelastic descriptions.[31] However, this conclusion might not be directly applicable to inhomogeneous ILT composition. Also with respect to the inhomogeneous ILT results, our study could only use idealized compositions of ILT. Although the developed analysis framework could easily process patient-individual ILT compositions, this information was not available for the present study. In addition, since vascular tissue properties are spatial inhomogeneous, a refined model should at least incorporate the gradual variation of properties between normal arterial and diseased (aneurysmal) tissues. Finally, it is also noted that our computations did not consider residual stresses (and strains) in zero-pressure configuration. Although well documented for healthy tissue, to the authors' best knowledge no adequate experimental residual stress data for AAA has been reported.

In summary, the present work aimed to explore the role played by ILT on stress distribution in AAAs using state-of-the-art modeling assumptions. The identified strong correlations of PWS with both ILT volume and minimum thickness of ILT layer underlined the importance played by ILT in the AAA wall stress distribution. Likewise, for all analyzed cases where ILT was present, the location of PWS coincided with the section of minimum ILT thickness, which demonstrated the significance played by ILT topology, i.e., geometrical configuration with respect to the arterial wall. Finally, ILT heterogeneity, i.e., the spatial composition of soft and stiff thrombus tissue can also considerably influence stress in AAA, helping to reveal possible failing mechanisms associated with ILT tissue that may increase the risk of aneurysm rupture. Therefore, we recommended considering this information for a biomechanical analysis of AAA. The present study is limited to the identification of influential biomechanical factors, and how its findings translate to an AAA rupture risk assessment remains to be explored by clinical studies.

ACKNOWLEDGMENT

We gratefully acknowledge Dr. F. Labruto for his assistance in the segmentation process.

CONFLICT OF INTEREST

T.C.G. is shareholder of VASCOPS GmbH, which should not have caused any conflict of interest for the present work. F.R., J.F.R., and G.M. have no conflict of interest issues.

REFERENCES

[1]Auer, M., and T. C. Gasser. Reconstruction and finite element mesh generation of abdominal aortic aneurysms from computerized tomography angiography data with minimal user interactions. *IEEE Trans Med. Imaging* 29:1022–1028, 2010.

[2]Ayyalasomayajula, A., J. P. Vande Geest, and B. R. Simon. Porohyperelastic finite element modeling of abdominal aortic aneurysms. *J. Biomech. Eng*. 132:104502, 2010.

[3]DiMartino, E. S., A. Bohra, J. P. Vande Geest, N. Gupta, M. S. Makaroun, and D. A. Vorp. Biomechanical properties of ruptured versus electively repaired abdominal aortic aneurysm wall tissue. *J. Vasc. Surg*. 43:570–576, 2006.

[4]DiMartino, E., S. Mantero, F. Inzoli, G. Melissano, D. Astore, R. Chiesa, and R. Fumero. Biomechanics of abdominal aortic aneurysm in the presence of endoluminal thrombus: experimental characterisation and structural static computational analysis. *Eur. J. Vasc. Endovasc. Surg*. 15:290–299, 1998.

[5]DiMartino, E. S., and D. A. Vorp. Effect of variation in intraluminal thrombus constitutive properties on abdominal aortic aneurysm wall stress. *Ann. Biomed. Eng*. 31(7):804–809, 2003.

[6]Doyle, B., A. Callanan, and T. McGloughlin. A comparison of modelling techniques for computing wall stress in abdominal aortic aneurysms. *Biomed. Eng. OnLine* 6:38, 2007.

[7]Elger, D. F., D. M. Blackketter, R. S. Budwig, and K. H. Johansen. The influence of shape on the stresses in model abdominal aortic aneurysms. *J. Biomech. Eng*. 118:326–332, 1996.

[8]Fillinger, M. F., M. L. Raghavan, S. P. Marra, J. L. Cronenwett, and F. E. Kennedy. In vivo analysis of mechanical wall stress and abdominal aortic aneurysm rupture risk. *J. Vasc. Surg*. 36:589–597, 2002.

[9]Gasser, T. C. An irreversible constitutive model for fibrous soft biological tissue: a 3-D microfiber approach with demonstrative application to abdominal aortic aneurysms. *Acta Biomater*. 7(6):2457–2466, 2011.
[10]Gasser, T. C., M. Auer, F. Labruto, J. Swedenborg, and J. Roy. Biomechanical rupture risk assessment of abdominal aortic aneurysms: model complexity versus predictability of finite element simulations. *Eur. J. Vasc. Endovasc. Surg*. 40:176–185, 2010.
[11]Gasser, T. C., G. Görgülü, M. Folkesson, and J. Swedenborg. Failure properties of intraluminal thrombus in abdominal aortic aneurysm under static and pulsating mechanical loads. *J. Vasc. Surg*. 48:179–188, 2008.
[12]Gasser, T. C., A. Nchimi, J. Swedenborg, J. Roy, N. Sakalihasan, D. Böckler, and A. Hyhlik-Dürr. A novel strategy to translate the biomechanical rupture risk of abdominal aortic aneurysms to their equivalent diameter risk: method and retrospective validation. *Eur. J. Vasc. Endovasc. Surg*. 47:288–295, 2014.
[13]Georgakarakos, E., C. V. Ioannou, Y. Kamarianakis, Y. Papaharilaou, T. Kostas, E. Manousaki, and A. N. Katsamouris. The role of geometric parameters in the prediction of abdominal aortic aneurysm wall stress. *Eur. J. Vasc. Endovasc. Surg*. 39:42–48, 2010.
[14]Georgakarakos, E., C. V. Ioannou, Y. Papaharilaou, T. Kostas, D. Tsetis, and A. N. Katsamouris. Peak wall stress does not necessarily predict the location of rupture in abdominal aortic aneurysms. *Eur. J. Vasc. Endovasc. Surg*. 39:302–304, 2010.
[15]Georgakarakos, E., C. V. Ioannou, S. Volanis, Y. Papaharilaou, J. Ekaterinaris, and A. N. Katsamouris. The influence of intraluminal thrombus on abdominal aortic aneurysm wall stress. *Int. Angiol*. 28:325–333, 2009.
[16]Hans, S. S., O. Jareunpoon, M. Balasubramaniam, and G. B. Zelenock. Size and location of thrombus in intact and ruptured abdominal aortic aneurysms. *J. Vasc. Surg*. 41:584–588, 2005.
[17]Harter, L. P., B. H. Gross, P. W. Callen, and R. A. Barth. Ultrasonic evaluation of abdominal aortic thrombus. *J. Ultrasound Med*. 1:315–318, 1982.
[18]Heng, M. S., M. J. Fagan, J. W. Collier, G. Desai, P. T. McCollum, and I. C. Chetter. Peak wall stress measurement in elective and acute abdominal aortic aneurysms. *J. Vasc. Surg*. 47:17–22, 2007.
[19]Hinnen, J.-W., O. H. J. Koning, M. J. T. Visser, and H. J. Van Bockel. Effect of intraluminal thrombus on pressure transmission in the abdominal aortic aneurysm. *J. Vasc. Surg*. 42:1176–1182, 2005.
[20]Inzoli, F., F. Boschetti, M. Zappa, T. Longo, and R. Fumero. Biomechanical factors in abdominal aortic aneurysm rupture. *Eur. J. Vasc. Surg*. 7:667–674, 1993.
[21]Karkos, C. D., U. Mukhopadhyay, I. Papakostas, J. Ghosh, G. J. L. Thomson, and R. Hughes. Abdominal aortic aneurysm: the role of clinical examination and opportunistic detection. *Eur. J. Vasc. Endovasc. Surg*. 19:299–303, 2000.
[22]Kazi, M., J. Thyberg, P. Religa, J. Roy, P. Eriksson, U. Hedin, and J. Swedenborg. Influence of intraluminal thrombus on structural and cellular composition of abdominal aortic aneurysm wall. *J. Vasc. Surg*. 38:1283–1292, 2003.
[23]Larsson, E., F. Labruto, T. C. Gasser, J. Swedenborg, and R. Hultgren. Analysis of aortic wall stress and rupture risk in patients with abdominal aortic aneurysm with a gender perspective. *J. Vasc. Surg*. 54:295–299, 2011.
[24]Li, Z.-Y., J. U-King-Im, T. Y. Tang, E. Soh, T. C. See, and J. H. Gillard. Impact of calcification and intraluminal thrombus on the computed wall stresses of abdominal aortic aneurysm. *J. Vasc. Surg*. 47:928–935, 2008.
[25]Limet, R., N. Sakalihassan, and A. Albert. Determination of the expansion rate and incidence of ruptur of abdominal aortic aneurysms. *J. Vasc. Surg*. 14:540–548, 1991.
[26]Maier, A., M. W. Gee, C. Reeps, J. Pongratz, H. H. Eckstein, and W. A. Wall. A comparison of diameter, wall stress, and rupture potential index for abdominal aortic aneurysm rupture risk prediction. *Ann. Biomed. Eng*. 38:3124–3134, 2010.
[27]Mower, W. R., W. J. Quiñones, and S. S. Gambhir. Effect of intraluminal thrombus on abdominal aortic aneurysm wall stress. *J. Vasc. Surg*. 26:602–608, 1997.
[28]Nissen, R., G. J. Cardinale, and S. Udenfriend. Increased turnover of arterial collagen in hypertensive rats. *Proc. Natl. Acad. Sci*. 75:451–453, 1978.
[29]O'Leary, S. A., E. G. Kavanagh, P. A. Grace, T. M. McGloughlin, and B. J. Doyle. The biaxial mechanical behaviour of abdominal aortic aneurysm intraluminal thrombus: classification of morphology and the determination of layer and region specific properties. *J. Biomech*. 47:1430–1437, 2014.
[30]Parr, A., M. McCann, B. Bradshaw, A. Shahzad, P. Buttner, and J. Golledge. Thrombus volume is associated with cardiovascular events and aneurysm growth in patients who have abdominal aortic aneurysms. *J. Vasc. Surg*. 53:28–35, 2011.
[31]Polzer, S., T. C. Gasser, B. Markert, J. Bursa, and P. Skacel. Impact of poroelasticity of intraluminal thrombus on wall stress of abdominal aortic aneurysms. *Biomed. Eng. OnLine* 11:62, 2012.
[32]Polzer, S., T. C. Gasser, J. Swedenborg, and J. Bursa. The impact of intraluminal thrombus failure on the mechanical stress in the wall of abdominal aortic aneurysms. *Eur. J. Vasc. Endovasc. Surg*. 41:467–473, 2011.
[33]Powell, J. T. Final 12-year follow-up of surgery versus surveillance in the UK small aneurysm trial. *Br. J. Surg*. 94:702–708, 2007.
[34]Raut, S. S., S. Chandra, J. Shum, and E. Finol. The role of geometric and biomechanical factors in abdominal aortic aneurysm rupture risk assessment. *Ann. Biomed. Eng*. 41:1459–1477, 2013.
[35]Riveros, F., S. Chandra, E. Finol, T. C. Gasser, and J. F. Rodriguez. A pull-back algorithm to determine the unloaded vascular geometry in anisotropic hyperelastic AAA passive mechanics. *Ann. Biomed. Eng*. 41:694–708, 2013.
[36]Rodríguez, J. F., G. Martufi, M. Doblaré, and E. A. Finol. The effect of material model formulation in the stress analysis of abdominal aortic aneurysms. *Ann. Biomed. Eng*. 37:2218–2221, 2009.
[37]Rodríguez, J. F., C. Ruiz, M. Doblaré, and G. A. Holzapfel. Mechanical stresses in abdominal aortic aneurysms: influence of diameter, asymmetry, and material anisotropy. *J. Biomech. Eng*. 130:021023, 2008.
[38]Sakalihasan, N., R. Limet, and O. D. Defawe. Abdominal aortic aneurysm. *Lancet* 365:1577–1589, 2005.
[39]Shum, J., G. Martufi, E. Di Martino, C. Washington, J. Grisafi, S. C. Muluk, and E. A. Finol. Quantitative assessment of abdominal aortic aneurysm geometry. *Ann. Biomed. Eng*. 39:277–286, 2011.
[40]Speelman, L., G. W. H. Schurink, E. M. H. Bosboom, J. Buth, M. Breeuwer, F. N. van de Vosse, and M. H. Jacobs.

The mechanical role of thrombus on the growth rate of an abdominal aortic aneurysm. *J. Vasc. Surg*. 51:19–26, 2009.
[41]Spencer, A. J. M. Continuum Theory of the Mechanics of Fibre-Reinforced Composites. New York: Springer, 1985.
[42]Stenbaek, J., B. Kalin, and J. Swedenborg. Growth of thrombus may be a better predictor of rupture than diameter in patients with abdominal aortic aneurysms. *Eur. J. Vasc. Endovasc. Surg*. 20:466–469, 2000.
[43]Thubrikar, M. J., F. Robicsek, M. Labrosse, V. Chervenkoff, and B. L. Fowler. Effect of thrombus on abdominal aortic aneurysm wall dilation and stress. *J. Cardiovasc. Surg. (Torino)* 44:67–77, 2003.
[44]Tierney, Á. P., A. Callanan, and T. M. McGloughlin. Use of regional mechanical properties of abdominal aortic aneurysms to advance finite element modeling of rupture risk. *J. Endovasc. Ther*. 19:100–114, 2012.
[45]Upchurch, G. R., and T. A. Schaub. Abdominal aortic aneurysm. *Am. Fam. Physician* 73:1198–1204, 2006.
[46]Vande Geest, J. P., M. S. Sacks, and D. A. Vorp. The effects of aneurysm on the biaxial mechanical behavior of human abdominal aorta. *J. Biomech*. 39:1324–1334, 2006.
[47]Vande Geest, J. P., M. S. Sacks, and D. A. Vorp. A planar biaxial constitutive relation for the luminal layer of intraluminal thrombus in abdominal aortic aneurysms. *J. Biomech*. 39:2347–2354, 2006.
[48]Venkatasubramaniam, A., T. Mehta, I. Chetter, J. Bryce, P. Renwick, B. Johnson, A. Wilkinson, and P. McCollum. The value of abdominal examination in the diagnosis of abdominal aortic aneurysm. *Eur. J. Vasc. Endovasc. Surg*. 27:56–60, 2004.
[49]Vorp, D. A., P. C. Lee, D. H. J. Wang, M. S. Makaroun, E. M. Nemoto, S. Ogawa, and M. W. Webster. Association of intraluminal thrombus in abdominal aortic aneurysm with local hypoxia and wall weakening. *J. Vasc. Surg*. 34:291–299, 2001.
[50]Wang, D. H. J., M. Makaroun, M. W. Webster, and D. A. Vorp. Mechanical properties and microstructure of intraluminal thrombus from abdominal aortic aneurysm. *J. Biomech. Eng*. 123:536–539, 2001.
[51]Wang, D. H. J., M. S. Makaroun, M. W. Webster, and D. A. Vorp. Effect of intraluminal thrombus on wall stress in patient-specific models of abdominal aortic aneurysm. *J. Vasc. Surg*. 36:598–604, 2002.